Wetting morphologies at microstructured surfaces

– Supporting information –

Ralf Seemann[1†], **Martin Brinkmann**[2‡], **Edward J. Kramer**[1], **Frederick F. Lange**[1], **and Reinhard Lipowsky**[2*]

[1] *Mitsubishi Chemical Center for Advanced Materials, UCSB, CA 93106, USA*

[2] *Max–Planck–Institute of Colloids and Interfaces, 14424 Potsdam, Germany* [§]

This supporting information contains three sections about experimental procedures, theoretical results for liquid filaments and wedges, and grooves with different cross–sections.

S1. Experimental procedures

In order to construct topographically microstructured surfaces with a certain wettability, we used the following procedures. Using standard photolithographic methods with pulsed ion gas etching, silicon substrates were topographically structured with surface grooves of rectangular cross–section, see Figure S1.

More precisely, five different samples were fabricated, each of which contained four or six distinct surface domains which differed in the aspect ratio X of their grooves. Taken together, these five samples provided 23 different aspect ratios in the range $0.04 \leq X \leq 0.60$.

The silicon wafers, which are covered by a thin SiO_x layer, were then cleaned and coated by a self–assembled monolayer. Both cleaning and coating were performed in a class 100 clean room. Degreasing of the wafers was done with ultrasonic cleaning in ethanol, acetone, and toluene. Residual hydrocarbons were etched away by a 30 min dip in fresh 1:1 H_2SO_4 (concentrated)/ H_2O_2 (30%) solution. The acids were removed by a thorough rinse in hot Millipore water. Finally, the surface energy of the clean substrate was modified by covering the surface with a self assembled monolayer of semifluorinated trichlorosilanes, $F(C_2F)_8(CH_2)_2SiCl_3$ purchased from Gelest, Tullytown, PA,

[†]Present Address: Max–Planck–Institute of Dynamics and Selforganization, Postfach 2353, 37018 Göttingen, Germany

[‡]Present Address: Interdisciplinary Research Institute Lille, 59652 Villeneuve d'Ascq, France

[*]Author for correspondence

[§]http://www.mpikg.mpg.de/th/

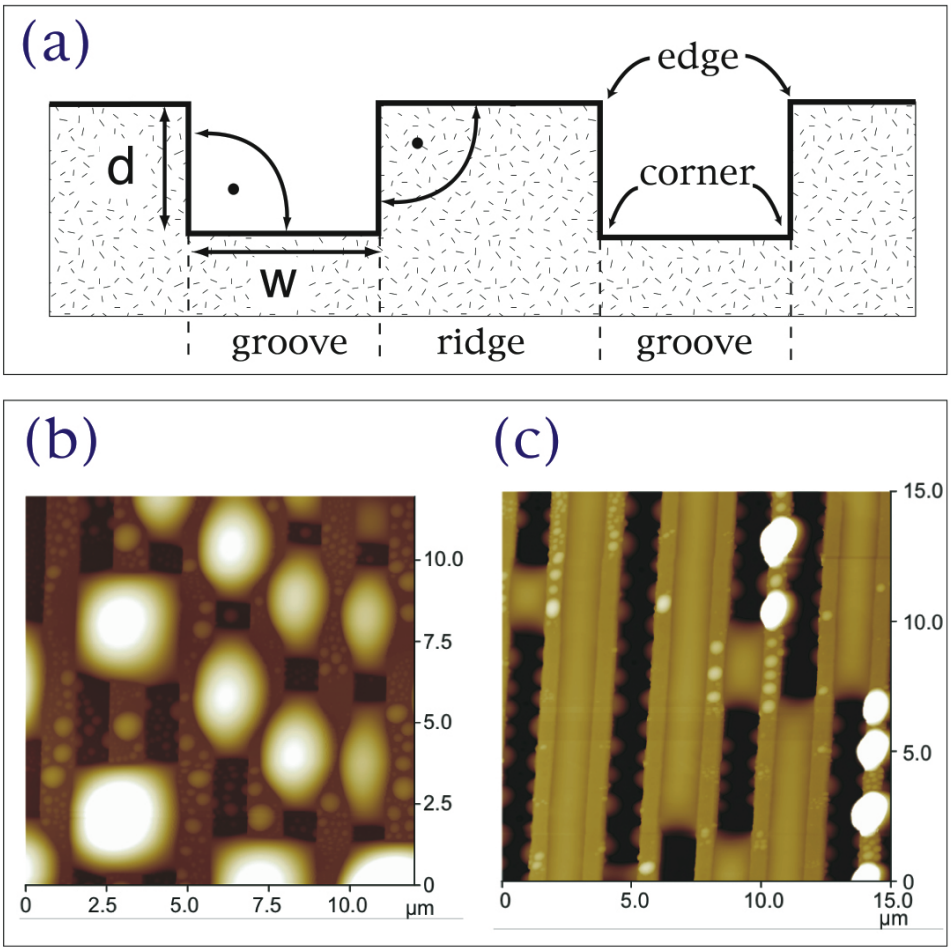

Figure S1: (a) Side view of the surface topography which consists of rectangular grooves separated by rectangular ridges. Each groove has depth d and width w which defines its aspect ratio $X \equiv d/w$. (b, c) AFM images of condensation patterns on grooved substrate with (b) groove aspect ratio $X = 0.18 \pm 0.01$ and material contact angle $\theta = 71 \pm 1$ deg and (c) $X = 0.46 \pm 0.02$ and $\theta = 67 \pm 3$ deg. In (b), the liquid forms large droplets (white) overlying the grooves and separated by essentially empty groove segments (dark stripes); the ridges separating the grooves have the same width as the grooves. In (c), the liquid forms extended filaments (light) within the grooves separated by groove segments (dark stripes) which contain rows of smaller droplets along the two corners at the groove bottom; the width of the ridges is half the width of the grooves.

USA. These molecules were deposited onto the silicon substrates from the vapor phase.

In order to fine tune the wettability, an additional treatment by oxygen plasma was performed which reduces the coverage of the trichlorosilanes and/or partially oxidizes the monolayer. In this way, various surface domains were prepared which had a contact angle θ for short chain polystyrene between $\theta = 5$ deg and $\theta = 80$ deg corresponding to the clean silicon substrate and to the complete trichlorosilane monolayer, respectively. The treatment is expected to create some surface heterogeneities since the oxygen plasma may not attack the groove sidewalls as strongly as the groove bottom.

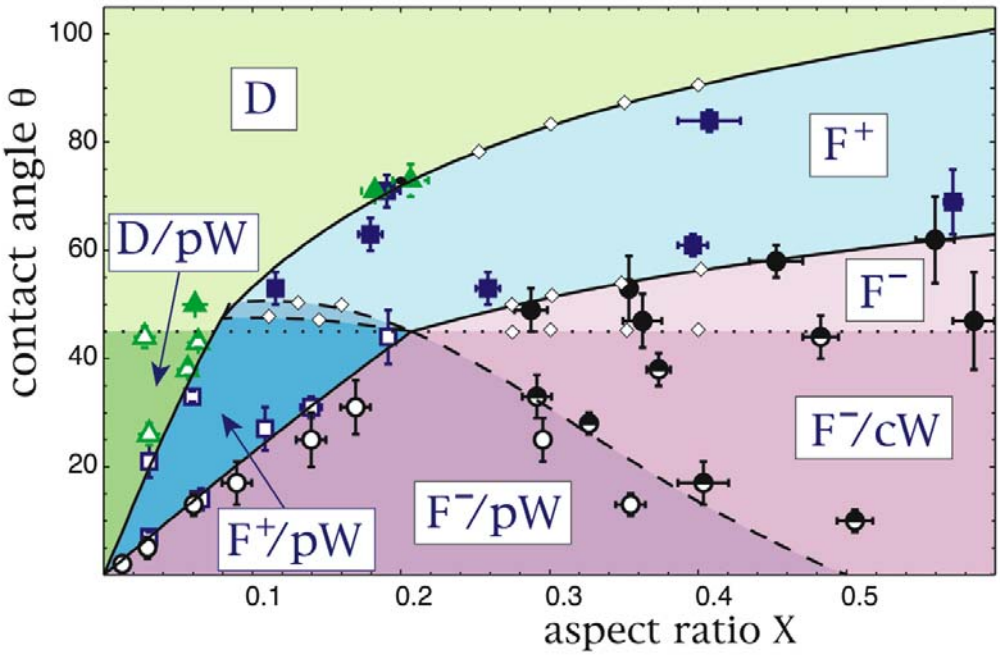

Figure S2: Morphology diagram as a function of groove aspect ratio X and material contact angle θ. This diagram contains seven different regimes which involve liquid droplets (D), filaments (F), pinned wedges (pW) and corner wedges (cW) as determined theoretically and as explained in Figure 4 of the main text. In addition, experimental data points (solid, open, and half–filled with error bars) corresponding to 41 out of 185 AFM scans have also been incluced. All 185 experimentally determined shapes are fully consistent with the theoretical classification.

The liquid structures were created by exposing the substrates for 6–48 hours to over-saturated vapor of short chain polystyrene (Polystyrene Mw = 2 kg/mol, Mw/Mn = 1.06, purchased from Pressure Chemical Company, Pittsburg, PA and Polystyrene Mw = 1.89 kg/mol, Mw/Mn = 1.06, by Polymer Standards Service, Mainz, Germany). During this exposure time, the polystyrene vapor condenses on the substrate creating liquid morphologies. Since the condensation process is rather slow, the liquid structures have sufficient time to attain morphologies which are close to their equilibrium states.

Lowering the temperature below the glass transition temperature, the liquid structures 'freeze' and their shape can now be scanned by atomic force microscopy (AFM). Previous AFM studies have shown that this 'freezing' process has no detectable influence on the morphology of the liquid. [1] In this way, we determined 185 individual liquid structures corresponding to droplets, filaments, wedges, and combinations thereof. 41 out of these 185 AFM scans have been included in the morphology diagram shown in Figure S2.

For a given surface domain, the contact angle was determined for several condensed morphologies. For each liquid morphology, the contact angle was measured at several contact line positions on the ridges, groove side walls, and groove bottom. An average was taken over about 20 contact angle values

obtained in this way. The variance (or dispersion) of these data was of the order of a few degrees as reported in Figure 1 of the main text and in the morphology diagram shown in Figure S2.

In general, one expects some contact angle hysteresis corresponding to the difference between advancing and receding contact angles. Since the liquid morphologies were formed by condensation, the measured contact angles are likely to represent advancing contact angles. However, as more liquid volume is condensed in a groove, the liquid structures merge and reorganize which could involve also some receding parts. The small variance of the measured contact angle seems to indicate that the contact angle hysteresis was small as well.

For the electrowetting experiments, the preparation procedure was slightly modified. In these experiments, one needs an insulating layer which acts as a capacitor between the conducting liquid and the conducting solid substrate. In the case of silicon, this insulating layer is provided by a layer of SiO_2. In order to create such an oxide layer, the silicon wafers were oxidized at a temperature of about 1000° C. The substrate surface was then coated with a self–assembled monolayer of OTS (Octadecyle–trichlorosilane). This monolayer was deposited onto the silicon wafer from solution.

S2. Analytical theory for liquid filaments and wedges

S2.1 Regime (F+): Liquid filaments without wedges

For contact angle $\theta > 45$ deg, one experimentally observes extended filaments which have a constant cross–section apart from the two segments close to the two end caps. Thus, the main body of the filament can be characterized by the filament angle θ_F as in the inset of Figure S3. This filament angle is uniquely determined by the groove aspect ratio X and by the substrate contact angle θ. We now derive an explicit expression for this functional relationship by using the approximation that we ignore the precise shape of the filament end caps and replace the real filament by one which has constant cross–section throughout. This approximation becomes very accurate in the limit of long filaments as one would intuitively expect and as one can check by explicit numerical calculation of the three–dimensional filament shapes.

In principle, one could achieve such a uniform filament state even experimentally if one 'sandwiched' the filament between two pistons which provide two confining walls orthogonal to it as shown in Figure S3. If the contact angle on these walls is equal to 90 deg, the cross–section of the filament will indeed be uniform.

If the liquid filament is in mechanical equilibrium in the absence of external forces, the total force which it exerts onto one of these pistons must vanish. This force consists of two contributions: the Laplace pressure which acts over the whole area of the filament cross–section and the interfacial tensions which act along the boundaries of this cross–section. Alternatively, one may also vary the liquid free energy with respect to the filament length for fixed filament

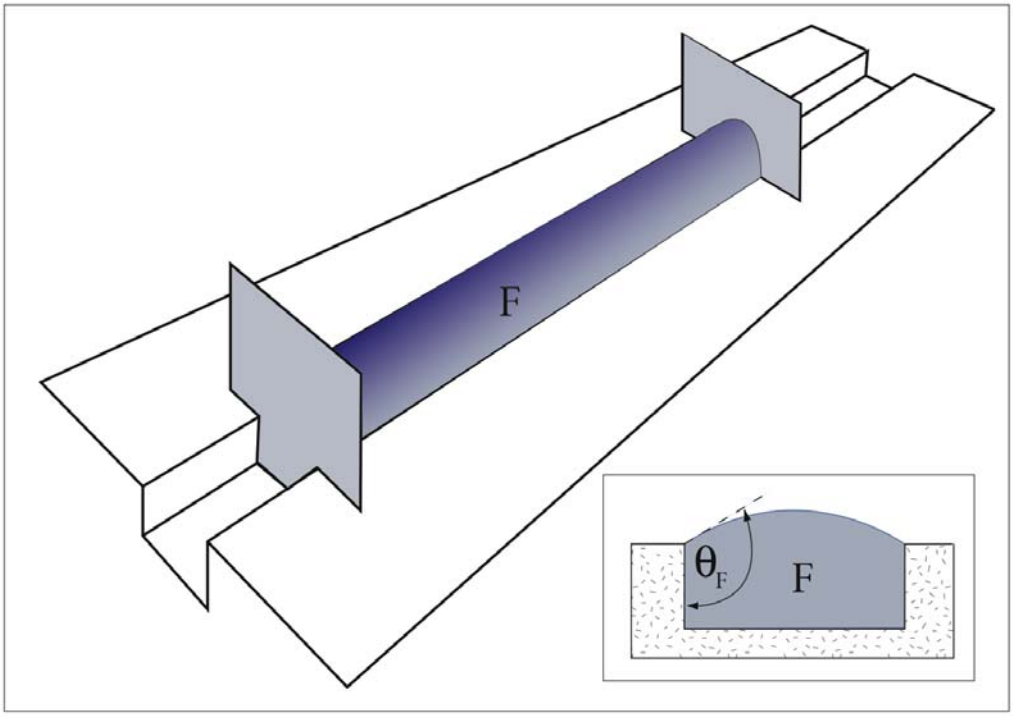

Figure S3: Liquid filament (F) in surface groove 'sandwiched' between two pistons which provide walls orthogonal to the long axis of the filament. The contact angle at these walls is 90 deg which ensures that the filament has constant cross–section and is bounded by a cylindrical meniscus. In mechanical equilibrium, the total force exerted by the filament onto each piston wall must vanish. The inset shows the filament cross–section and the associated filament angle $\theta_{\rm F}$.

volume in order to find the filament with minimal free energy, a calculation method which was previously used for chemically patterned surfaces [2]. Both methods are equivalent and lead, after some computation, to the functional relationship

$$(2X+1)\cos(\theta) = \frac{90\ \text{deg} - \theta_{\rm F}}{2\cos(\theta_{\rm F})} + \frac{\sin(\theta_{\rm F})}{2} + 2X\cos(\theta_{\rm F}) \qquad \text{(S.1)}$$

between the aspect ratio X, the contact angle $\theta > 45$ deg of the underlying substrate, and the filament angle $\theta_{\rm F}$. This equation can be explicitly solved for θ or X and has a unique solution for $\theta_{\rm F}$ in the physically meaningful range $\theta < \theta_{\rm F} < \theta + 90°$.

As soon as the contact angle $\theta_{\rm F}$ exceeds the limiting value $\theta + 90$ deg, the contact line segments along the groove edges become unpinned, and the extended filament is transformed into an overspilling droplet. Thus, the 'fattest' filaments are given by $\theta_{\rm F} = \theta + 90$ deg (this applies to the case in which the substrate contact angle $\theta \leq 90$ deg as considered here; for $\theta > 90$ deg, the 'fattest' filament corresponds to $\theta_{\rm F} = 180$ deg). When this value is inserted into the functional relationship (S.1), one obtains the filament instability line $X = X_*(\theta)$ with

$$X_*(\theta) \equiv \frac{\theta - \sin(\theta)\cos(\theta)}{4\sin(\theta)[\sin(\theta) + \cos(\theta)]} \qquad \text{(S.2)}$$

for $45\,\mathrm{deg} < \theta < 90\,\mathrm{deg}$.

For a filament with vanishing Laplace pressure, one has $\theta_\mathrm{F} = 90$ deg. If this value is inserted into (S.1), one finds that the aspect ratio X and the contact angle θ must satisfy the relation $X = X_0(\theta)$ with

$$X_0(\theta) \equiv \frac{1-\cos(\theta)}{2\cos(\theta)} \qquad \text{for} \quad \theta > 45 \text{ deg} \quad . \tag{S.3}$$

When this latter equation is solved for θ, one obtains the right part of equation (2) as given in the main text.

S2.2 Regime (F+/pW): Liquid filaments connected to wedges

For $\theta < 45$ deg, one has to include the forces arising from the liquid wedges along the groove corners. Thus, we now replace the intermediate liquid which forms the transition region between the filament and the two adjacent wedges by a piston which has the same length as this intermediate region. The force exerted by the filament onto the piston from one side must now balance the force exerted by the two wedges from the other side. This leads to another equation between the filament angle, groove aspect ratio, and substrate contact angle which replaces equation (S.1) and which is valid for $\theta < 45$ deg.

For the fattest filaments with $\theta_\mathrm{F} = \theta + 90$ deg, one now obtains the instability line

$$X_*(\theta) \approx \frac{\theta - \sin(\theta)\cos(\theta)}{8\sin(\theta)^2} \tag{S.4}$$

for small θ which represents a very good approximation for all $\theta < 45$ deg. Likewise, filaments with vanishing Laplace pressure and $\theta_\mathrm{F} = 90$ deg are formed if the aspect ratio X and the substrate contact angle θ satisfy

$$X = X_0(\theta) \equiv \frac{1-\cos(\theta)}{2\sin(\theta)} \qquad \text{for} \quad \theta < 45 \text{ deg}. \tag{S.5}$$

When this equation is solved for θ, one obtains the left part of equation (2) as given in the main text. For $\theta = 45$ deg, the two expressions (S.5) and (S.3) give the same value $X_0 = (\sqrt{2}-1)/2 = 0.207$.

S2.3 Stability of filaments with negative Laplace pressure

The functional relationship $\theta = \theta_0(X)$ defines a boundary line within the two–dimensional (X, θ)–plane. As one crosses this line, both the Laplace pressure and the free energy of the liquid filaments change sign. In fact, for $\theta > 45$ deg, the filament free energy F_F has the simple form

$$F_\mathrm{F} \approx P_\mathrm{sc} V \sin(\theta_\mathrm{F} - 90 \text{ deg}) \tag{S.6}$$

for large volumes V with the pressure scale $P_\mathrm{sc} \equiv (2\Sigma/w)$ which depends on interfacial tension Σ and groove width w. The Laplace pressure of the filament is then given by $P_\mathrm{La} = \partial F_\mathrm{C}/\partial V \approx P_\mathrm{sc}\sin(\theta_\mathrm{F} - 90 \text{ deg})$.

Inspection of equation (S.6) shows that the free energy is positive for filament angle $\theta_F > 90$ deg but *negative* for $\theta_F < 90$ deg. In contrast, large droplets always have a positive free energy. This has the remarkable consequence that extended filaments with $\theta_F \leq 90$ deg, which are formed in grooves with $\theta \leq \theta_0(X)$, are globally stable even for large volumes since they represent the states of lowest free energy. This global stability extends to filaments with small positive Laplace pressure. As this positive pressure exceeds a certain threshold value which depends on the liquid volume, the filaments become metastable and the state of lowest free energy is given by overspilling droplets.

S2.4 The appearance and disappearance of wedges

The stability criterion of Concus and Finn [3] implies that filaments, which are shorter than the groove, must be connected to wedges in the groove corners provided $\theta < 45$ deg. It is now interesting to ask how these wedges appear or disappear as one varies the contact angle from $\theta < 45$ deg to $\theta > 45$ deg or vice versa.

First, let us consider the initial morphology (D/pW) for contact angle $\theta < 45$, i.e., an overspilling droplet which is connected to wedges. As one subsequently increases the contact angle, these wedges shrink until they disappear at $\theta = 45$ deg. This behavior is continuous and reversible. Thus, if one starts initially at $\theta > 45$ deg with a droplet (D) without wedges and now decreases the contact angle θ, wedges with infinitesimal cross–section appear and start to grow as soon as one has crossed the boundary line $\theta = 45$ deg.

The same continuous growth and shrinkage of the wedges is found along the boundary line $\theta = 45$ deg for $X > (\sqrt{2} - 1)/2 \simeq 0.207$. In the latter case, the liquid attains the morphologies (F–/cW) and (F–) for $\theta < 45$ deg and $\theta < 45$ deg, respectively, corresponding to filaments with *negative* Laplace pressure.

In contrast, for filaments with *positive* Laplace pressure, wedges disappear in a discontinuous fashion. This leads to a small range of θ values above $\theta > 45$ deg for which filaments (F+/pW) with wedges and filaments (F+) without wedges can coexist. This coexistence region corresponds to the shaded area in Figure S4. The upper boundary of this region, which extends up to about 52 deg, represents the instability line for the morphologies (F+/pW). As one reaches this line from below, the wedges recede from the groove edges and then undergo the classical Rayleigh–Plateau instability because of their positive Laplace pressure. On the other hand, if one starts from a filament state (F+), this state remains essentially unchanged as one decreases the contact angle until one reaches the lower boundary of the shaded coexistence region in Figure S4. At this latter boundary line, wedges start to protrude from the filament. Numerical minimization of the liquid free energy indicates that this protrusion process corresponds to a 'soft mode' of the system, i.e., that a filament with short wedges has essentially the same free energy as a filament with long wedges. Experimentally, these latter states are difficult to find since (i) they occur only at the instability line for the filament states (F+), and (ii)

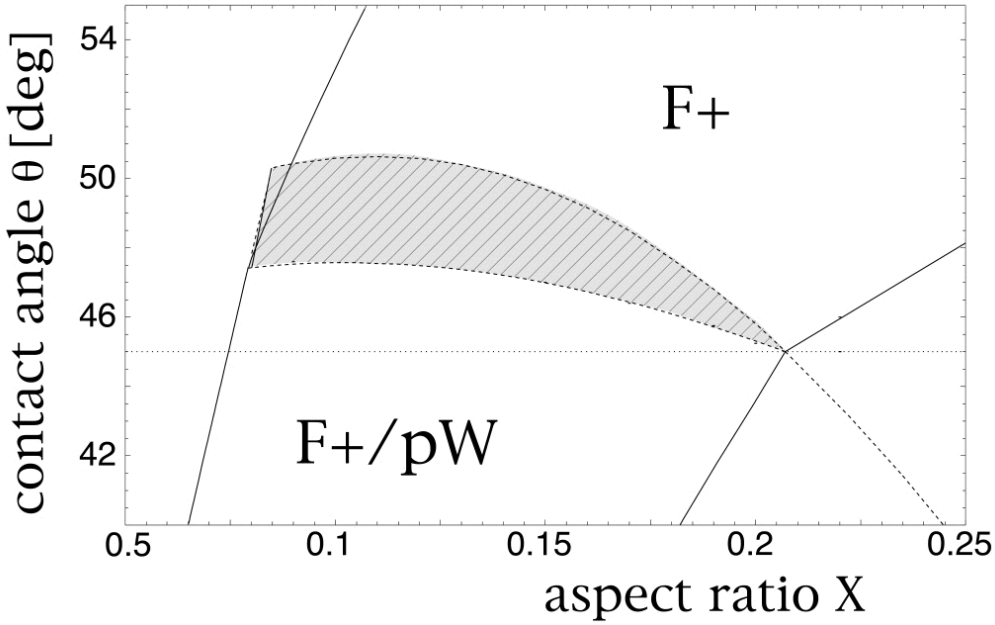

Figure S4: The coexistence region (shaded) of the liquid morphologies (F+/pW) and (F+) corresponding to filaments with and without wedges, respectively. As one increases the contact angle θ, the morphology (F+/pW) remains stable up to the upper boundary of the shaded region. As one decreases θ, the morphology (F+) becomes unstable at the lower boundary of this region.

they are easily perturbed and pinned by adsorbed impurities or surface defects.

S3. Grooves with different cross–sections

So far, we have discussed grooves with rectangular cross–section. In this case, both the opening angle ω_c of the groove corner and the opening angle ω_e of the groove edge are equal to 90 deg as shown in Figure S5. A change in these two opening angles is useful in order to suppress liquid wedges and to increase the stability of liquid filaments.

In general, the corner opening angle ω_c of the groove determines the contact angle regime for which the liquid forms wedges along the groove corners. It follows from the general stability criterion of Concus and Finn [3] that the liquid will form wedges along the groove corners provided $\theta < \theta_{\rm W}(\omega_c)$ with the boundary angle

$$\theta_{\rm W} \equiv (180 \text{ deg} - \omega_c)/2 \quad . \tag{S.7}$$

For the overall morphology diagram in the (X, θ)–plane, all four shape regimes with wedges lie below the horizontal line $\theta = \theta_{\rm W}$. Thus, *in order to suppress wedges, one should increase the opening angle ω_c of the groove corners.* This property was first discussed by Shuttleworth and Bailey [4] for grooves with triangular cross–section and a corner opening angle $\omega_c = 180\,\text{deg} - 2\psi$ which implies $\theta_{\rm W} = \psi$.

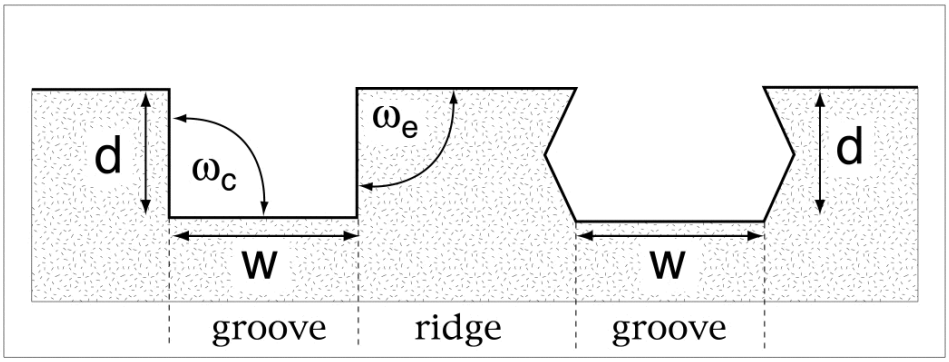

Figure S5: Side view of the surface topography which consists of grooves separated by ridges. The opening angle of the groove corner is denoted by ω_c, the opening angle of the groove edge by ω_e. For the rectangular cross–section on the left, both opening angles are identical and equal to 90 deg; for the hexagonal cross–section on the right, one has $\omega_c > 90$ deg and $\omega_e = 180$ deg $- \omega_c < 90$ deg.

The edge opening angle ω_e, on the other hand, determines the contact angle range for which the contact line stays pinned to the groove edge. The shape regimes of stable filaments grow in the overall morphology diagram as one increases this range of pinned contact angles. If the contact line is pinned to an edge with opening angle ω_e, the corresponding contact angle $\theta_{\rm p}$ can vary in the range

$$\theta \leq \theta_{\rm p} \leq \theta + 180 \text{ deg} - \omega_e \quad . \tag{S.8}$$

For the overall morphology diagram in the (X, θ)–plane, the filament regimes (F+) and (F-) shrink or grow as one decreases or increases this contact angle range for θ_p, i.e., as one increases or decreases the edge opening angle ω_e. In fact, the filament regime (F-) is lost completely if one increases the edge opening angle beyond the threshold value $\omega_e^* \equiv 180 - \theta$. Thus, *in order to increase the stability of filaments, one should decrease the edge opening angle* ω_e.

For rectangular cross–sections, both opening angles are equal to 90 deg. If one wants to change the cross–section in such a way that liquid wedges are further suppressed and, at the same time, liquid filaments become more stable, one has to simultaneously *increase* the corner opening angle above 90 deg and to *decrease* the edge opening angle below 90 deg. A simple example which fulfills both conditions is provided by a hexagonal cross–section with $\omega_c = 120$ deg and $\omega_e = 60$ deg. If the groove width w is now defined by the width of the groove bottom, the cross–sectional area is equal to $wd + \sqrt{3}d^2/6$.

For such a hexagonal cross–section, the wedge boundary angle has the value $\theta_{\rm W} = 30$ deg and the range of pinned contact angles is given by $\theta \leq \theta_{\rm p} \leq \theta + 120$ deg. Using the analytic approach described above, one can again calculate the boundary line of the overall morphology diagram which corresponds to filaments with zero Laplace pressure. One then finds that this boundary line

is given by $X = X_0(\theta)$ with

$$X_0(\theta) \equiv \frac{\sqrt{3}}{4} \frac{1 - \cos(\theta)}{\cos(\theta)} \qquad \text{for} \quad \theta > \theta_{\rm W} = 30 \text{ deg}. \tag{S.9}$$

The smallest aspect ratio for which the groove supports an extended filament at zero Laplace pressure with no wedges attached is given by $X = X_0(\theta_{\rm W})$. For grooves with hexagonal cross–section, one has $X = X_0(\theta_{\rm W} = 30 \text{ deg}) = (2 - \sqrt{3})/4 = 0.067$ as follows from equation (S.9). For grooves with rectangular cross-section, the corresponding value is given by $X_0(\theta_{\rm W} = 45 \text{ deg}) = (\sqrt{2} - 1)/2 = 0.207$ as follows from the expression (S.3). Thus, grooves with hexagonal cross–sections lead to extended filaments (without wedges) which are stable both for smaller values of the groove aspect ratio X and for smaller values of the substrate contact angle θ as compared to grooves with rectangular cross–sections.

Finally, let us briefly mention another method to improve the stability of filaments which is provided by additional chemical modification of the topographically structured substrates. If the grooves are characterized by the contact angle θ as before but the ridges are more lyophobic and, thus, have a larger contact angle $\theta_{\rm r} > \theta$, the range of possible filament angles $\theta_{\rm F}$ is given by $\theta < \theta_{\rm F} < \theta_{\rm r} + 90$ deg for $\theta_{\rm r} < 90$ deg and by $\theta < \theta_{\rm F} < 180$ deg for $\theta_{\rm r} > 90$ deg. This explicitly shows that the filament stability is optimized if one makes the difference $\theta_{\rm r} - \theta$ as large as possible.

References

[1] Seemann, R., Herminghaus, S. & Jacobs, K. (2001) Phys. Rev. Lett. **87**, 196101/1–196101/4.

[2] Brinkmann, M. & Lipowsky, R. (2002) J. Appl. Phys. **92**, 4296–4306.

[3] Concus, P. & Finn, R. (1969) Proc. Natl. Acad. Sci. U.S.A. **63**, 292–299.

[4] Shuttleworth, R. & Bailey, G. L. J. (1948) , Disc. Faraday Soc. **3**, 16–22.